ELSEVIER

Earth and Planetary Science Letters 146 (1997) 243–258

EPSL

Basaltic liquids and harzburgitic residues in the Garrett Transform: a case study at fast-spreading ridges

Yaoling Niu [a,*], Roger Hékinian [b]

[a] *Department of Earth Sciences, The University of Queensland, Brisbane, Queensland 4072, Australia*
[b] *IFREMER, Centre de Brest, DRO / GM, B.P. 37, 29287 Plouzané, France*

Received 9 May 1996; revised 28 October 1996; accepted 30 October 1996

Abstract

The peridotite–basalt association in the Garrett Transform, ~13°28′S, East Pacific Rise (EPR), provides a prime opportunity for examining mantle melting and melt extraction processes from both melts and residues produced in a common environment beneath fast-spreading ridges. The peridotites are highly depleted, clinopyroxene-poor, harzburgites. Residual spinel, orthopyroxene and clinopyroxene in these harzburgites are extremely depleted in Al_2O_3, and plot at the most depleted end of the abyssal peridotite array defined by samples from slow-spreading ridges (including samples from hotspot-influenced ridges), suggesting that these harzburgites are residues of very high extents of melting. The residual peridotites from elsewhere at the EPR (i.e., Hess Deep and the Terevaka Transform) also are similarly depleted. This suggests that the extent of melting beneath the EPR is similar to, or even higher than, beneath ridges influenced by hotspots (e.g., Azores hotspot in the Atlantic Ocean and Bouvet hotspot in the Indian Ocean), and is significantly higher than $\leq 10\%$, a value that has been advocated to be the average extent of melting beneath global ocean ridges. Many of these harzburgite samples, however, show whole-rock incompatible element abundances higher than expected. These same samples also have various amounts of excess olivine with forsterite contents as low as Fo_{85}. The total olivine modes correlate inversely with olivine forsterite contents, and positively with whole-rock incompatible element abundances. These correlations suggest that the excess olivine and incompatible element enrichment are both the result of melt–solid re-equilibration. The buoyant melts that ascend through previously depleted residues crystallize olivine at shallow levels as a result of cooling. Entrapment of these melts leads to whole-rock incompatible element enrichment. These observations contrast with the notion that melts formed at depth experience little low pressure equilibration during ascent.

Keywords: harzburgite; mid-ocean ridge basalts; East Pacific Rise; mantle; melts; mid-ocean ridges

1. Introduction

Abyssal peridotites and mid-ocean ridge basalts (MORB) are complementary products of mantle melting and melt extraction processes that create the ocean crust. Studies of abyssal peridotites [1–4] and MORB showed that the extent of mantle melting is high beneath hotspot-influenced shallow ridges, and is low beneath deep ridges away from hotspots. These results have led to the recognition of global correlation of MORB chemistry with ridge axial depth and crustal thickness [5], and the notion that mantle temperature variation exerts the primary control on the extent of melting beneath global ocean

* Corresponding author. Tel.: +61 7 3365 2372. Fax: +61 7 3365 1277. E-mail: niu@earthsciences.uq.edu.au

PII S0012-821X(96)00218-X

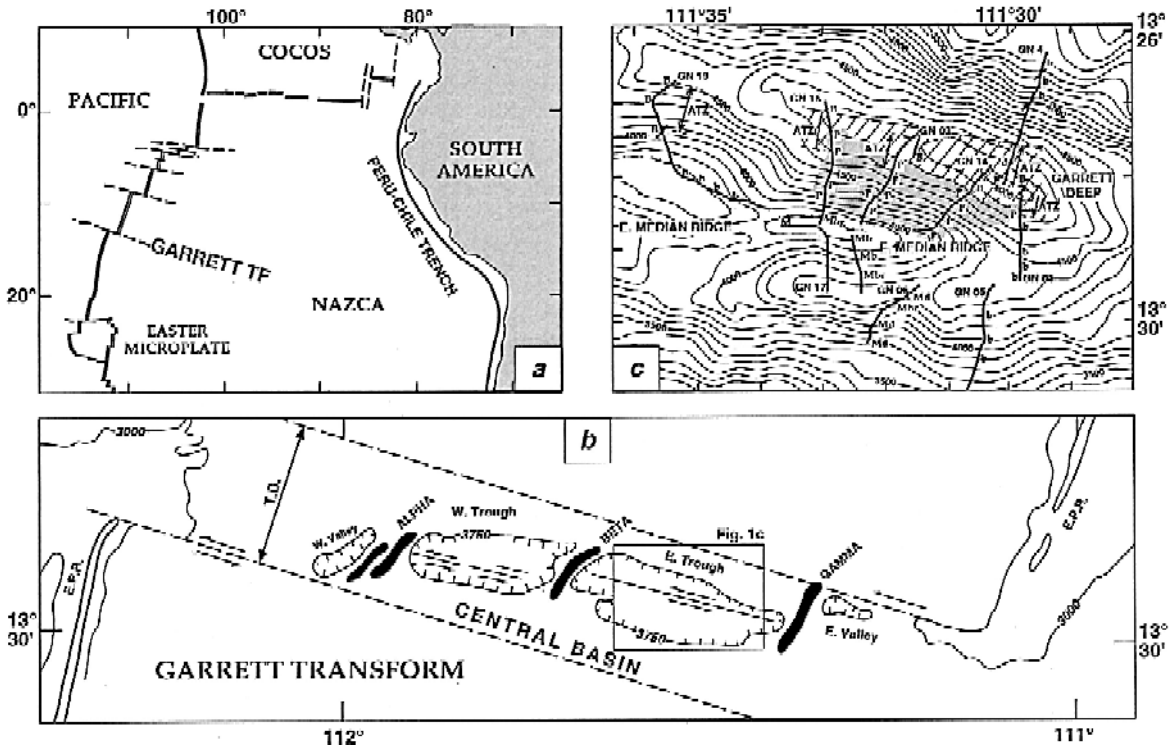

Fig. 1. (a) Location of the Garrett Transform offsetting the EPR at ~13°28′S. (b) Morphotectonic representation of the Garrett Transform showing the volcanic ridges (Alpha, Beta, and Gamma) and transform troughs [17,18]. (c) A detailed bathymetry (100 m intervals) of the Garrett Deep and northern flank of the East Median Ridge showing the extent of the outcrop of peridotite–basalt association (shaded area). The thick lines are diving tracks (e.g., GN 01, GN 03, etc.). GS 03 is the track of a deep-towed bottom camera run. The samples studied are from dives GN 03, GN 04, GN 13, GN 14 and GN 15. The observed lithologies are: fresh (*B*) and altered (*b*) basalt flows, consolidated and metamorphosed breccia (*Mbr*), metabasalt (*Mb*), and serpentinized peridotites (*P*).

ridges [2,5–8]. This conclusion is, however, based largely on data from slow-spreading ridges in the Atlantic and Indian Oceans. At the fast-spreading East Pacific Rise (EPR), there is little correlation between MORB chemistry and ridge depth [8–11], and EPR MORB show chemical systematics that differ from those at slow-spreading ridges on both regional and ridge segment scales [8–12]. Clearly, an improved understanding of EPR MORB genesis requires petrological data on both residual peridotites and associated basalts. However, there had been no detailed sampling of peridotites from the EPR [13,14] until very recent submersible [15–20] and drilling [21] investigations at Hess Deep, and the Garrett and Terevaka transforms.

In this paper, we present geochemical data on

Notes to Table 1:

[a] *Im* = impregnation; total volume of impregnation veins/veinlets were estimated on board. Thin-section chips and analyzed portions of harzburgite samples are fresh cuttings away from impregnation veinlets and hydration haloes.

[b] The reported mineral modes (vol%) were obtained by point-counting at 1 mm intervals based on one or two thin sections for each sample, and are partially reconstructed. We assigned all textural serpentines, whether or not they have olivine psedomorphs, and associated magnetite (abundant) to the serpentine (Serp) category; optically fresh (unaltered) olivine, either as individual grains/aggregates or as ''meshes'' surrounded or veined by serpentine, to olivine (Ol); unaltered orthopyroxene, spatially associated bastite pseudomorphs and peripheral talc to primary orthopyroxene (Opx); unaltered clinopyroxene and associated tremolitic amphiboles to primary clinopyroxene (Cpx); spinel with or without magnetite rims to primary spinel (Sp).

Table 1
Garrett transform sample descriptions

Sample	Depth	Setting	Sample size	Sample description	Im [a]	Modes of samples analysed [b]					Counts
	(m)		(cm)	(On board)	(vol%)	Serp	Ol	Opx	Cpx	Sp	(total)
Serpentinized harzburgite											
GN3-9	4324	Outcrop on a scarp	25×29×13	Harzburgite; no impregnation	0	79.15	4.40	15.00	nil	1.45	2000
GN14-1	5050	Talus	20×18×18	Harzburgite; 4 gabbroic veinlets (2–5 mm thick)	8	71.80	10.16	15.24	0.85	1.95	1237
GN14-2	5046	Talus	13×15×15	Harzburgite; 1 gabbroic veinlet (< 2 mm thick)	10	83.89	8.71	6.62	0.70	0.08	1230
GN14-5	4908	Outcrop	12×14×12	Harzburgite; no impregnation	0	49.29	39.88	9.47	0.22	1.14	1710
GN14-7	4833	Talus	40×40×15	Harzburgite; 1 gabbroic veinlet (~ 2 mm thick)	1	73.92	7.31	17.36	0.30	1.12	2007
GN14-9	4660	Outcrop	16×16×5	Harzburgite; no impregnation	0	49.76	37.18	11.69	0.16	1.21	1237
GN14-14	4244	Outcrop	30×20×9	Harzburgite; 3 gabbroic veinlets (2–10 mm thick) and 1 dikelet (3 mm thick)	20	74.01	11.65	13.07	0.24	1.03	1263
GN15-2	4647	Talus, flank of the ridge	15×17×17	Dunite; no impregnation	0	68.27	22.97	7.41	nil	1.35	1258
GN15-5	4688	Outcrop, flank of the ridge	17×10×10	Harzburgite; no impregnation	0	83.49	0.34	14.50	nil	1.68	1205
GN15-10	4217	Outcrop	21×12×8	Harzburgite; no impregnation	0	51.87	22.37	24.27	0.08	1.41	1212
Diabase											
GN4-3	4602	Talus, active tectonic zone	25×20×15	Plagioclase–olivine phyric, ~ equal amounts plagioclase and clinopyroxene, plus trace of olivine and magnetite							
GN4-9	4013	Outcrop	28×20×20	Metamorphosed, aphyric, ~ equal amounts plagioclase and clinopyroxene in groundmass							
GN13-9	3764	Talus	40×20×8	Aphyric, equal amounts plagioclase and clinopyroxene plus trace olivine and opaque							
GN15-4	4697	Talus, flank of the ridge	26×16×10	Aphyric, equal amounts plagioclase and clinopyroxene plus ~ 3% opaque							
Basalt											
GN4-1	5062	Talus, active tectonic zone	25×20×20	Pillow fragment; aphyric glass							
GN4-11	3720	Outcrop, dikes	20×10×10	Pillow fragment; aphyric glass							
GN13-1	4528	Outcrop	20×15×15	Sheet flow; plagioclase–olivine basaltic glass							
GN13-6	3657	Outcrop	25×25×12	Pillow fragment; aphyric glass							
GN13-8	3764	Talus	40×20×15	Pillow fragment; aphyric non-glassy basalt							
GN15-1	4801	Talus, Central Basin	28×14×12	Pillow fragment; olivine–phyric glass							

peridotites and spatially associated basaltic samples from the Garrett Transform. This peridotite–basalt association allows, for the first time, a close examination of mantle melting and melt extraction processes from both melts and residues produced in a common environment at the EPR. Also, this study is the first attempt at whole-rock trace element systematics of abyssal peridotites, and will be a useful addition to the geochemical data base for models concerning MORB genesis and chemical geodynamics in general.

2. Geological background

The Garrett Transform is associated with the fastest (145 mm/yr) [22] strike-slip motion on the Earth, and offsets the EPR at 13°28′S by 130 km [23] (Fig. 1a). This transform is one of the few transforms in which active volcanism is observed [17–20,24], and mantle peridotites are recovered [13,14,17–20] at the EPR. Previous studies of some dredged samples from this transform [25,26] warranted an in situ observation by the submersible *Nautile* [17]. In the Garrett Transform, active volcanism is primarily taking place along three parallel ridges oblique to the transform strike, but fresh lavas also exist at deep locations near the peridotite outcrops (Fig. 1b). Mantle peridotites are exposed as an ~10 km long sliver in the transform valley and along the northern flank of the median ridge (Fig. 1c). Gabbros occur as a dike complex within the peridotite domain, and diabasic dikes of variable thickness are common. The peridotites are variously serpentinized, and are locally impregnated with basaltic veins/veinlets of variable thickness (< 1 mm to a few centimetres).

3. Samples and analytical techniques

Field occurrence, hand specimen characteristics, and petrography of the samples studied are summarized in Table 1. These include 10 serpentinized harzburgites; 4 fresh diabases; 1 fresh non-glassy basalt; and 5 fresh glassy basalts. The analyzed portions of harzburgites are fresh cuttings away from impregnation veinlets and seafloor weathering haloes. Major element compositions of residual minerals in harzburgites and basaltic glasses were analyzed using a Camebax SX 50 microprobe at IFREMER [18]. Whole-rock major elements for non-glass basalts, diabases and harzburgites, and Cr and Ni for harzburgites were analyzed by XRF at The University of Queensland following [27,28]. Trace elements (except for Cr and Ni in harzburgites) were analyzed using a FISONS PQ inductively coupled plasma mass spectrometer at The University of Queensland. The whole-rock analytical data and uncertainties for repeated analyses of reference standards PCC-1 and BIR-1 for trace elements are given in Table 2. We have determined 37 trace elements for all the samples but we report here rare-earth elements, Y, Zr, Nb, Hf, Ta, and Th, because all other elements are observed to be mobile during serpentinization. Sample preparation and analytical procedure can be obtained from the authors and are described in an **EPSL Online Background dataset** [1].

4. Data and interpretations

4.1. Basaltic liquids

Fig. 2 shows that the large range of incompatible element abundances in basaltic samples can be explained by various extents of fractional crystallization from a compositionally similar parent (Fig. 2a–d). This is better described by glass samples (liquid compositions). The inflected trend on CaO/Al_2O_3 vs. MgO plot (Fig. 2c) defined by glass samples suggests that crystallization follows the sequence of olivine → olivine + plagioclase → olivine + plagioclase + clinopyroxene. The different abundance levels on chondrite-normalized rare-earth element (REE) diagrams (Fig. 2e–f) are consistent with varying extents of fractional crystallization (Fig. 2d). The overall parallel REE patterns suggest that their parental melts may have formed by similar extents of melting of a similarly depleted fertile mantle. By assuming a fertile mantle that is slightly more depleted than source for average MORB (see caption

[1] http://www.elsevier.nl/locate/epsl (mirror site USA, http://www.elsevier.com/locate/epsl)

of Fig. 2), the primary melts parental to these basaltic liquids can be explained by $\geq 20\%$ melting by either the batch (Fig. 2g) or fractional (Fig. 2h) melting model. While the extent of melting calculated using incompatible trace elements alone is subject to large errors, due to source compositional uncertainties, this calculated value is nevertheless comparable with $23 \pm 2\%$ melting calculated from major elements ($Na_8 \approx 2.23 \pm 0.09\%$ and $Ca_8/Al_8 \approx 0.87 \pm 0.01$) [7].

4.2. Harzburgitic residues

4.2.1. Mineral modes and whole-rock major element compositions

Fig. 3a shows that, compared with abyssal peridotites from slow-spreading ridges [4,29,30], Garrett peridotites are extremely depleted harzburgites with clinopyroxene (cpx) being essentially absent. This suggests that these harzburgites are residues of high extents of melting. Also, these harzburgites have variable and high abundances of ''total modal olivine'' (olivine + serpentine). The apparent high olivine modes could be over-estimated because orthopyroxene (opx) is often subject to serpentinization as well [31], and volume expansion is often associated with serpentinization. However, petrography shows that serpentinization is primarily after olivine in these harzburgites (see note to Table 1), which is also evident from the inverse correlation between olivine and serpentine modes (Fig. 3b). Note that the correlation in Fig. 3b is not due to data closure because the opx mode is not constant. The observation that olivine pseudomorphs are preserved in most samples suggests that the effect of volume expansion on the estimated olivine mode can be neglected for this purpose. Importantly, the significant inverse correlation of ''total olivine'' modes with olivine forsterite (Fo) contents (Fig. 3c) demonstrates the presence of excess olivine in these harzburgites prior to serpentinization. The excess olivine, by its variable and low Fo contents, is inconsistent with being a residual phase, but is consistent with being crystallized from a basaltic melt. In terms of whole-rock major element compositions, the high FeO contents in these harzburgites (Table 2) are largely controlled by the presence of excess olivine of low Fo content (Fig. 3d). Therefore, these harzburgites are not simple residues.

4.2.2. Major element compositions of residual minerals

It has been demonstrated that $Cr^{\#}$ ($= Cr/[Cr + Al]$) in spinel and Al_2O_3 contents in opx and cpx of residual peridotites are sensitive indicators of the extent of melting [1,3,32,33] because Al is a moderately incompatible element and its abundances in these phases decrease with progressive melting. Fig. 4 shows that these minerals in Garrett harzburgites are extremely depleted in Al_2O_3, and plot at the most depleted end of the abyssal peridotite array defined by samples from slow-spreading ridges (i.e., the Mid-Atlantic Ridge and Southwest Indian Ocean Ridge). Note that Garrett residual minerals are as depleted as, or even more depleted than, peridotites from hotspot-influenced ridges (points 5–7). Comparison with melting residues produced by peridotite melting experiments [32], the highly depleted residual mineral compositions and the point close to cpx exhaustion (Fig. 3a) suggests that these harzburgites are residues of $\sim 25\%$ melting. This high extent of melting is comparable to that estimated from major and REE abundances in the associated basaltic liquids (see above), but is significantly higher than $\leq 10\%$, a value that has been advocated as the average extent of melting beneath global ocean ridges [34,35].

4.2.3. Whole-rock minor and trace element systematics

We have demonstrated that Garrett harzburgites are not simple residues, but residues of very high extents of melting (Fig. 3aFig. 4) that have been modified with additional olivine with low Fo content (Fig. 3c). The low-Fo olivine can only be explained by its crystallization from a cooling melt. The signature of such a melt component is well preserved in the whole-rock incompatible element compositions (Fig. 5). The whole-rock incompatible element abundances correlate positively with ''total olivine'' modes (Fig. 5a) and inversely with olivine Fo contents (Fig. 5b–d). These correlations, which are inconsistent with melting, but consistent with refertilization of a melt, indicate that both excess olivine and elevated abundances of incompatible elements in these harzburgites are the consequence of the same melt–solid equilibration process. Buoyant melts that ascend through previously depleted melting residues

Table 2
Major and trace element analyses of harzburgites, diabases and basalts from the Garrett Transform

Sample:	3-9 Harz	14-1 Harz	14-2 Harz	14-5 Harz	14-7 Harz	14-9 Harz	14-14 Harz	15-2 Harz	15-5 Harz	15-10 Harz	PCC-1	RSD (%)	4-3 Dbs	4-9 Dbs	13-8 Bslt	13-9 Dbs	15-4 Dbs	4-1 Glass	4-11 Glass	13-1 Glass	13-6 Glass	15-1 Glass	BIR-1	RSD (%)
Weight percent by XRF													**Weight percent by microprobe**											
SiO_2	39.76	39.54	43.85	40.10	41.41	40.64	39.90	38.48	36.47	42.43			51.00	50.28	50.78	50.83	49.07	50.78	50.13	50.58	50.47	50.50		
TiO_2	0.05	0.05	0.06	0.10	0.02	0.08	0.06	0.05	0.07	0.02			1.17	1.27	2.05	2.25	1.09	1.25	1.11	1.16	1.73	2.45		
Al_2O_3	0.60	0.72	0.75	0.69	0.58	0.93	0.69	0.76	0.45	0.53			14.76	14.21	13.48	12.69	15.25	14.17	15.40	15.59	14.73	14.96		
FeOt	8.64	10.58	9.64	11.15	7.92	10.36	10.15	12.10	13.28	8.30			9.96	9.88	11.76	12.63	8.97	9.81	9.07	8.95	10.15	10.07		
MnO	0.06	0.13	0.16	0.16	0.11	0.15	0.13	0.12	0.13	0.12			0.18	0.18	0.20	0.21	0.19	0.19	0.19	0.16	0.14	0.15		
MgO	39.27	36.91	35.37	36.30	39.09	38.21	37.25	38.05	38.11	37.88			7.66	8.65	6.87	6.49	8.52	8.05	8.95	8.79	7.57	6.83		
CaO	0.10	1.24	3.01	1.23	0.79	0.78	0.90	0.20	0.15	0.2			12.68	11.30	11.31	11.51	12.94	12.29	12.24	12.34	11.27	10.26		
Na_2O	0.27	–	–	–	–	–	–	–	–	–			2.34	2.48	2.74	2.70	1.83	2.23	2.18	2.37	2.67	3.71		
K_2O	–	–	0.01	–	–	–	–	–	–	0.01			0.10	0.04	0.20	0.15	0.02	0.04	0.03	0.04	0.11	0.19		
P_2O_5	0	–	–	–	–	–	–	–	–	–			0.07	0.08	0.18	0.20	0.05	0.06	0.05	0.10	0.15	0.06		
LOI	10.87	10.04	6.21	9.80	9.11	8.18	10.86	9.53	10.54	10.33			–	0.98	0.09	–	1.34	–	–	–	–	–		
Total	99.63	99.20	99.06	99.54	99.04	99.33	99.94	99.28	99.19	99.82			99.91	99.36	99.67	99.66	99.26	100.24	99.35	100.09	98.99	99.18		
$Mg^{\#}$	89.0	86.1	86.7	85.3	89.8	86.8	86.7	84.9	83.6	89.1			60.46	3.45	3.6	50.5	65.3	61.9	66.2	66.1	59.6	57.3		
Parts per million (ppm) by XRF																								
Cr	2154	2168	2003	2430	2664	4034	3338	2320	1975	1962														
Ni	1847	1816	1634	1626	2218	2068	2116	1982	1776	2211														
Parts per million (ppm) by ICP–MS																								
Sc	9.64	10.5	11.6	17.8	9.2	10.3	9.48	6.91	7.14	9.29	8.65	3.9	36.6	39.8	39.2	44.8	37.5	36.4	26.4	33.3	36.3	35.9	43.5	1.6
V	24	28	31	50	23	32	24	13	24	21	23.32	0.8	260	264	335	379	245	255	193	235	302	331	283	3.5
Cr	–	–	–	–	–	–	–	–	–	–	–	–	137	224	232	272	425	372	317	394	330	307	373	3.1
Co	107	113	111	117	109	115	110	140	133	114	127	3.7	49	49	46	45	47	48	40	47	46	51	55	7.1
Ni	–	–	–	–	–	–	–	–	–	–	–	–	47	48	89	66	102	67	92	129	102	153	170	2.1
Ga	0.68	1.05	1.64	0.97	0.53	1.02	0.95	0.94	1.11	0.63	0.503	4.1	16	16.2	17.8	18.1	15.7	15.7	15.4	15.8	17.5	18.9	15.4	2.3
Y	0.48	0.99	1.18	1.85	0.22	0.88	1.18	0.68	1.90	0.12	0.079	7.9	24.0	24.9	40.1	43.3	23.0	22.6	18.3	22.6	34.2	45.6	13.5	2.4
Zr	0.39	0.96	1.88	0.80	0.12	1.37	2.27	0.57	1.64	0.03	0.192	6.5	48.3	56.4	117	125	42.5	49.1	36.0	46.3	98.1	131	13.1	2.0
Parts per billion (ppb) by ICP–MS													**Parts per million (ppm) by ICP–MS**											
Nb	11	8.8	16	12	8.2	14	12	7.6	68	6.1	42	17.5	0.92	1.12	3.13	3.30	0.86	0.93	0.57	0.77	2.44	2.05	0.54	1.2
La	25	37	72	73	13	45	40	538	59	37	32	7.6	1.41	1.81	3.99	4.14	1.37	1.42	0.98	1.24	3.18	3.61	0.58	3.4
Ce	29	106	169	218	16	86	124	93	278	110	57	3.3	5.02	6.33	13.01	13.59	5.03	5.01	3.55	4.63	10.61	12.89	1.84	1.7
Pr	4.7	21	30	38	2.8	19	27	16	70	17	8	14.7	1.00	1.23	2.40	2.52	1.02	0.98	0.72	0.96	1.97	2.48	0.38	1.8
Nd	33	125	180	225	15	118	166	77	465	71	28	14.1	5.55	6.56	12.18	12.98	5.64	5.36	4.10	5.39	10.11	13.07	2.24	1.7
Sm	17	53	78	115	6.4	55	76	29	203	13	7	26.7	2.23	2.47	4.24	4.54	2.24	2.05	1.64	2.15	3.54	4.68	1.02	1.5
Eu	40	26	41	55	3.5	23	28	8.3	13	30	2	49.5	0.88	0.95	1.47	1.57	0.89	0.82	0.66	0.87	1.25	1.55	0.49	1.7
Gd	31	90	136	210	13	93	126	55	287	14	8	34.1	3.22	3.51	5.72	6.27	3.17	2.94	2.39	3.09	4.81	6.39	1.67	3.2
Tb	7.8	19	26	41	2.8	19	24	12	51	2.3	2	28.8	0.59	0.63	1.02	1.11	0.57	0.55	0.44	0.57	0.85	1.15	0.32	2.6
Dy	68	145	195	326	27	140	188	96	344	16	12	7.8	4.20	4.41	7.12	7.73	4.03	3.82	3.12	3.96	5.95	8.01	2.38	2.2
Ho	18	34	44	71	8.7	32	40	25	72	4.2	3	21.0	0.88	0.92	1.48	1.61	0.84	0.81	0.66	0.83	1.23	1.67	0.52	2.4
Er	61	112	145	217	31	107	132	84	221	15	13	11.3	2.63	2.71	4.40	4.74	2.46	2.40	1.95	2.42	3.66	4.91	1.54	2.5
Tm	10	19	23	33	5.4	17	22	14	35	2.6	3	20.5	0.40	0.41	0.66	0.72	0.37	0.36	0.30	0.37	0.56	0.75	0.22	2.1
Yb	81	139	158	219	44	122	148	97	230	26	22	7.3	2.52	2.59	4.16	4.51	2.31	2.30	1.86	2.31	3.51	4.69	1.49	2.8
Lu	15	24	27	35	8.6	20	25	17	39	5.3	6	9.6	0.38	0.39	0.63	0.68	0.34	0.34	0.28	0.34	0.53	0.70	0.22	2.1
Hf	16	30	65	45	3.7	49	79	19	44	1.3	8	17.1	1.49	1.70	3.30	3.56	1.40	1.43	1.11	1.47	2.73	3.70	0.53	1.8
Ta	6.8	2.2	2.8	1.7	3.2	3.2	2.1	2.6	7.1	2.1	11	7.0	0.079	0.097	0.247	0.265	0.072	0.077	0.059	0.065	0.194	0.177	0.049	1.1
Th	1.3	1.8	2.5	1.6	1.4	1.6	3.8	1.6	8.1	1.8	10	9.8	0.045	0.057	0.189	0.200	0.040	0.044	0.030	0.037	0.148	0.111	0.030	6.6

crystallize olivine at shallow levels as a result of cooling. Entrapment of these melts raises the abundances of incompatible elements in the whole-rock harzburgites.

Fig. 6 shows chondrite-normalized REE abundances in the harzburgites. For comparison, model melting residues by batch (Fig. 6a) and fractional (Fig. 6b) melting also are shown. Obviously, both the abundance levels and patterns are inconsistent with their being simple melting residues. The abundance levels are variable and higher than expected given the similarly depleted residual mineral compositions in these harzburgites. The slopes for light REEs are too shallow for melting residues. Also, batch melting cannot in any way explain samples of low REE abundances (i.e., GN14-7 and GN15-10). Some samples show no obvious Eu anomalies, whereas others show either negative or positive Eu anomalies. Note that GN15-2 has anomalously high La, which, together with smaller La anomalies in several other samples, is interpreted as La being mobile during serpentinization. Any process that involves a melt would have affected Ce and Pr, at the very least, as well as La. Although the effects of plagioclase may be invoked to explain the Eu anomalies, the absence of plagioclase in the harzburgites analyzed does not support this interpretation. Given that Sr lacks any systematics in these rocks (not shown), it is possible that Eu, like Sr, may also be quite mobile during serpentinization. In any case, the overall patterns and variable abundance levels are consistent with refertilization of a melt (Fig. 5c).

4.2.4. Evaluation of the extent of refertilization

To evaluate precisely the extent of refertilization is not straightforward. However, the relative extent of refertilization can be estimated using REEs by adding a melt with composition similar to GN4-11 to residues of 25% fractional melting. Such a melt is chosen because: (1) all the Garrett basaltic liquids have similar REE patterns (Fig. 2e); (2) GN4-11 has only olivine on the liquidus (see Fig. 2c; olivine is the only phase observed to have crystallized from the refertilizing melt); and (3) GN4-11 has an $Mg^{\#}$ of $\sim 63.8–66.2$ (assuming $Fe^{3+}/[Fe^{3+}+Fe^{2+}] \approx 0–0.1$ in the melt), which would be in equilibrium with olivine of $Fo_{85.4-86.7}$, comparable to the observed excess olivine. A residue of 25% fractional melting is indicated by the near exhaustion of cpx (Fig. 3a) and highly depleted residual mineral compositions (Fig. 4), and batch melting cannot explain the low REE abundance samples (Fig. 6). The results are shown in Fig. 7a–c for representative light (Ce), intermediate (Tb), and heavy (Yb) REEs. The amount of GN4-11 (f) required to match the data varies from 0.1% to $\sim$ 12%. Note that the f values derived from REEs also explain the abundances of minor (TiO_2) and major (FeO) element variations, and olivine Fo contents in the harzburgites (Fig. 7d–f).

4.2.5. Issues on high field strength elements (HFSEs)

Fig. 8a–c plots primitive mantle normalized incompatible element abundances in the harzburgites. The patterns display several anomalous features concerning HFSEs. Not shown, Garrett basaltic liquids exhibit rather smooth patterns. Th is more depleted than Nb in the basaltic liquids, yet the opposite is observed in the harzburgites. Nb is more depleted than Ta in both liquids and harzburgites. A positive Ti anomaly exists in all but GN15-5 samples. While positive Zr–Hf anomalies are present in some harzburgites, the large negative anomalies in others are striking. Since the refertilization process discussed above affects Ti as well as the ''adjacent'' REEs (Fig. 7), positive Ti anomalies would have already existed prior to refertilization, which seems

Note to Table 2:

Harz = serpentinized harzburgite; Dbs = diabase; Bslt = non-glassy basalt; Glass = basaltic glass; FeOt = total Fe expressed as FeO; LOI = loss on ignition; $Mg^{\#} = Mg/[Mg + Fe^{2+}]$, assuming total FeO as Fe^{2+} for harzburgites, and 90% total FeO as Fe^{2+} for diabases and basalts. All the analyses are whole-rock compositions except for basaltic glasses. Major element data for glasses were analyzed at IFREMER using a Camebax SX 50 [18]. Whole-rock XRF analyses were done at the University of Queensland following [27,28]. Except for Cr and Ni in harzburgites, which were analyzed by XRF, all the trace elements were analyzed at the University of Queensland using a Plasma Quad Inductively coupled mass spectrometer (ICP–MS). PCC-1 = average of 6 repeated analyses of 2 digestions. BIR-1 = average of 18 repeated analyses of 12 digestions. %RSD is the relative standard deviations about the averages for PCC-1 and BIR-1. Sample preparation and analytical procedures can be obtained from the authors and are described in an **EPSL Online Background dataset**.

to be a common feature in highly depleted peridotites [36]. However, the anomalies associated with Zr–Hf and Nb–Ta need attention.

Zr–Hf anomalies: As Zr and Hf do not show anomalies in basalts, these anomalies in residual harzburgites are thus unexpected. Rampone et al. [37] interpreted the negative anomalies of Zr and Sr in an N-MORB type ophiolite from Internal Lig-

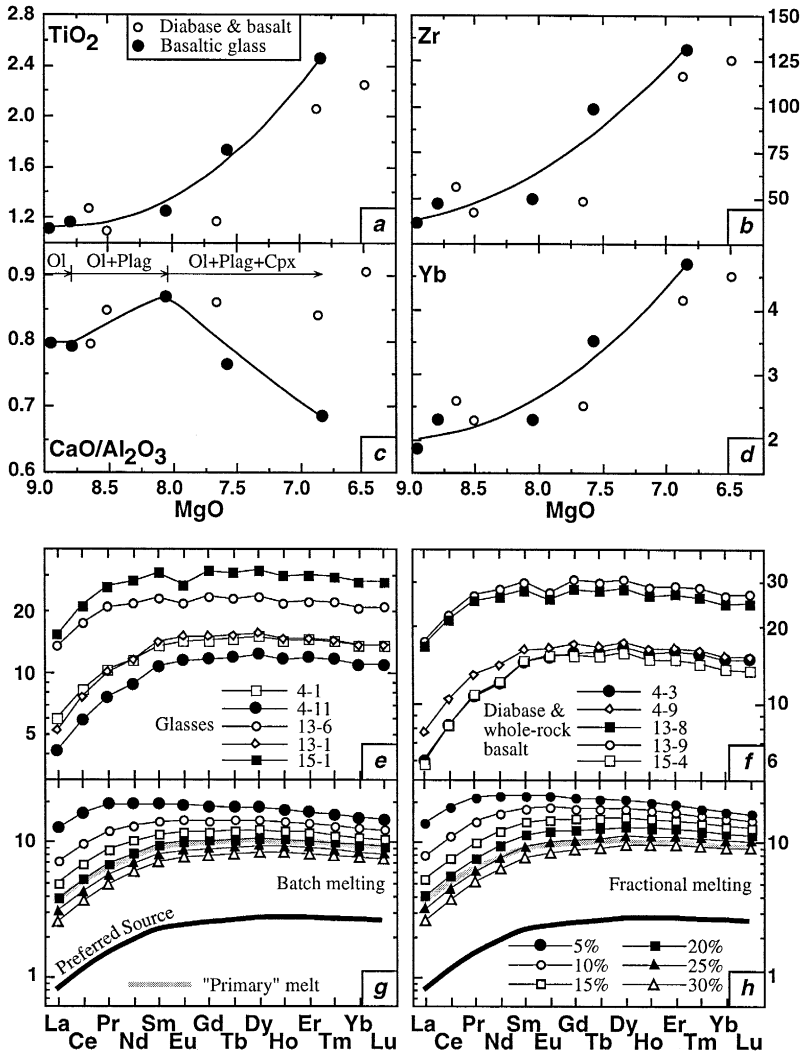

Fig. 2. (a)–(d) MgO variation diagrams of representative major, minor, and trace elements for Garrett basaltic rocks. (e) and (f) Chondrite–normalized [42] REE abundances for these basaltic rocks. (g) and (h) Comparisons of model melts by batch melting (g) and fractional melting (h) with a hypothetical primary melt parental to Garrett basaltic liquids (thick shaded line). The primary melt is approximated by adding 12% olivine to GN4-11 to be in equilibrium with mantle olivine Fo_{90} (i.e., the primary melt would have Mg# ≈ 72, assuming olivine/melt $K_d^{Fe-Mg} = 0.3$ [56]). The preferred fertile mantle source (thick solid line) is the average of R717, the least depleted, and R238, the moderately depleted, Ronda spinel lherzolites [57]; this choice was made because Garrett basaltic liquids are slightly more depleted than average N-type MORB, for which R717 is ideal [57]. This fertile mantle has subsolidus modes of 66% olivine (Ol), 24% orthopyroxene (Opx), 9% clinopyroxene (Cpx), and 2% spinel (Spl), but we have assumed high pressure modes of 55% Ol, 30% Opx, 13% Cpx, and 2% Spl following [58]. The melting modes are taken from the polybaric melting reaction of [52]: 0.464 Cpx + 0.681 Opx + 0.048 Spl ⇒ 0.193 Ol + 1 Melt. Mineral/liquid partition coefficients are given in Appendix A.

uride, North Italy, as reflecting ''changes in the relative magnitude of Zr, Sr, and REE partition coefficients, depending on specific melting conditions''. As Sr in Garrett harzburgites is quite mobile, whether Sr exhibits similar features prior to serpentinization is unknown. Since both positive (weak) and negative (strong) Zr–Hf anomalies are present (Fig. 8a–c), variation in melting condition may not be important. Both positive and negative Zr anomalies have been observed in melt inclusions in high-Mg olivine phenocrysts in basalts [38,39], and were interpreted as representing unmixed ''true'' instantaneous melt fractions. If so, this implies that ''microscale'' heterogeneities exist with respect to Zr and Hf in the mantle. The presence of a Zr–Hf rich phase in the fertile mantle is possible, but it is unlikely for it to survive in residues after $>20\%$ melting. As Garrett harzburgites have undergone melt refertilization, it is possible that such a Zr–Hf phase (ZrO_2–baddeleyite is a more likely candidate) may have co-precipitated with the excess olivine. If so, two possibilities exist: (1) uneven distribution of this phase in the harzburgites would lead to the observed Zr–Hf anomalies; (2) positive Zr–Hf anomalies may be expected in harzburgites [36], but large negative Zr–Hf anomalies may be due to incomplete digestion of this phase during sample preparation. A careful evaluation of these scenarios are warranted.

Nb–Ta fractionation, and the peculiar Nb–Th relationship: it has been widely accepted that Nb and Ta are geochemically identical, and that the Nb/Ta ratio is constant, and is close to chondritic values (16–18) in all oceanic basalts [40–42]. Very recent studies [43,44] have shown that Nb/Ta ratios in MORB are not constant, but vary significantly, from 18 in highly enriched lavas to as low as 9 in ex-

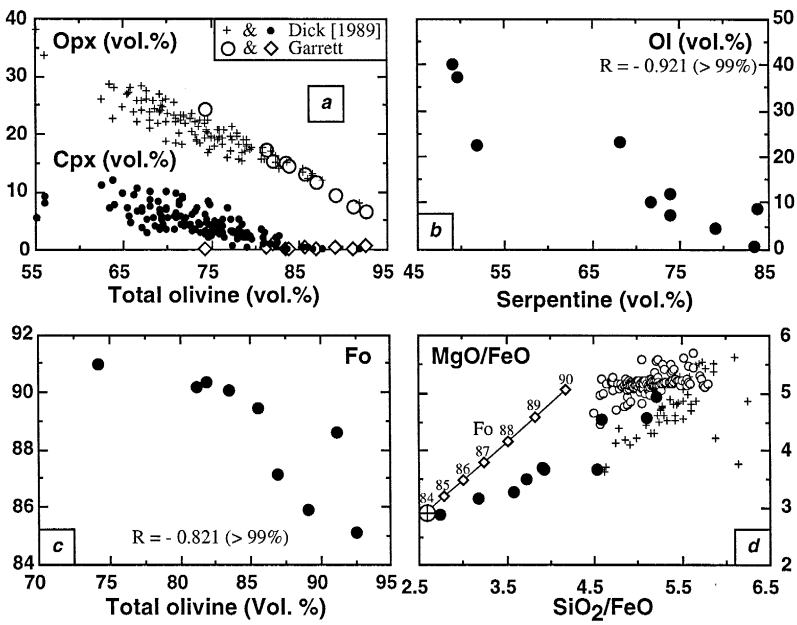

Fig. 3. (a) Orthopyroxene (opx) and clinopyroxene (cpx) modes are plotted against olivine modes to compare Garrett harzburgites with abyssal peridotites from slow-spreading ridges discussed by [4,29,30]. For Garrett harzburgites, the ''total olivine'' plotted is the sum of olivine and serpentine (see Table 1) modes. (b) Olivine modes correlate inversely with serpentine modes in Garrett harzburgites. (c) Olivine forsterite (Fo) contents inversely correlate with ''total olivine'' in Garrett harzburgites. (d) Relative to whole-rock analyses of abyssal peridotites from the Southwest Indian Ocean Ridge [59] and to reconstructed whole-rock abyssal peridotite compositions [52] using the published modes and mineral analyses of Dick [4,29,30], whole-rock Garrett harzburgites show low MgO/FeO and SiO_2/FeO ratios (high FeO; see Table 2), which are consistent with the presence of low-Fo olivine. The diamonds symbols are olivine compositions plotted for reference. Note that Garrett whole-rock compositions show MgO deficiency relative to SiO_2 (Table 2), perhaps due to MgO loss during serpentinization.

tremely depleted ones, indicating that Nb is more incompatible than Ta during melting. If so, one would expect even lower Nb/Ta ratios in residual harzburgites. This is indeed the case. Fig. 8f shows that the Nb/Ta ratio increases with increasing extent

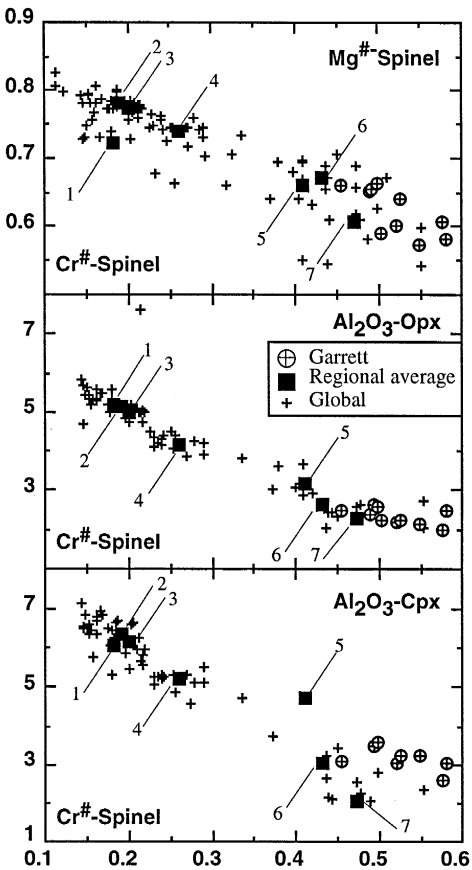

Fig. 4. In comparison, residual minerals in Garrett harzburgites plot at the most depleted end of the data array defined by those in abyssal peridotites from slow-spreading ridges [2,4,29,30,60,61]. These harzburgites are as depleted as, or even more depleted than, peridotites from hotspot-affected ridges (e.g., points 5–7). The Garrett mineral data are from samples with olivine Fo > 89, including new analyses of samples previously studied [25,26]. These indicate that, prior to olivine addition, Garrett harzburgites were residues of very high extents (~25%) of melting. The numbered symbols are regional averages: *1* = Atlantis II fault zone; *2* = Vulcan fault zone; *3* = Islas Orcadas fault zone; *4* = Bullard fault zone; *5* = Bouvet fault zone (near Bouvet hotspot) in the Indian Ocean; *6* = 15°N axial valley (near 14°N hotspot [62]); *7* = 43°N fault zone in the Atlantic (near Azores hotspot).

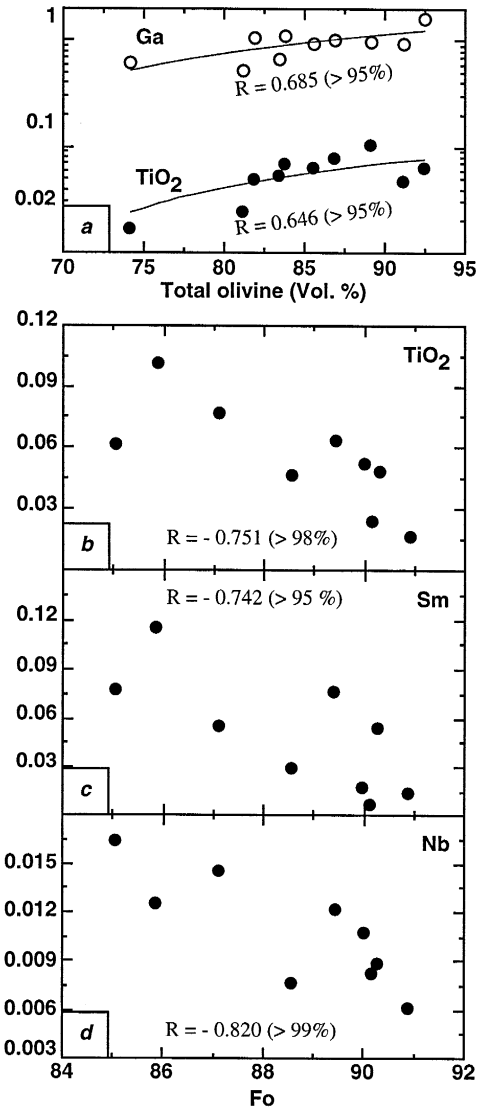

Fig. 5. (a) ''Total olivine'' modes correlate positively with incompatible element (e.g., Ga and Ti) abundances in Garrett harzburgites. (b)–(d) Olivine forsterite (Fo) contents in these harzburgites correlate inversely with incompatible element (e.g., TiO_2, Sm and Nb) abundances. The values in parentheses are confidence levels of the correlation coefficients. Note that no olivine is analyzed from sample GN15-2 due to almost complete serpentinization (see Table 1).

of refertilization, indicating that the Nb/Ta ratio in truly depleted residues unaffected by melt refertilization would be as low as 2. Given that Nb and Ta are

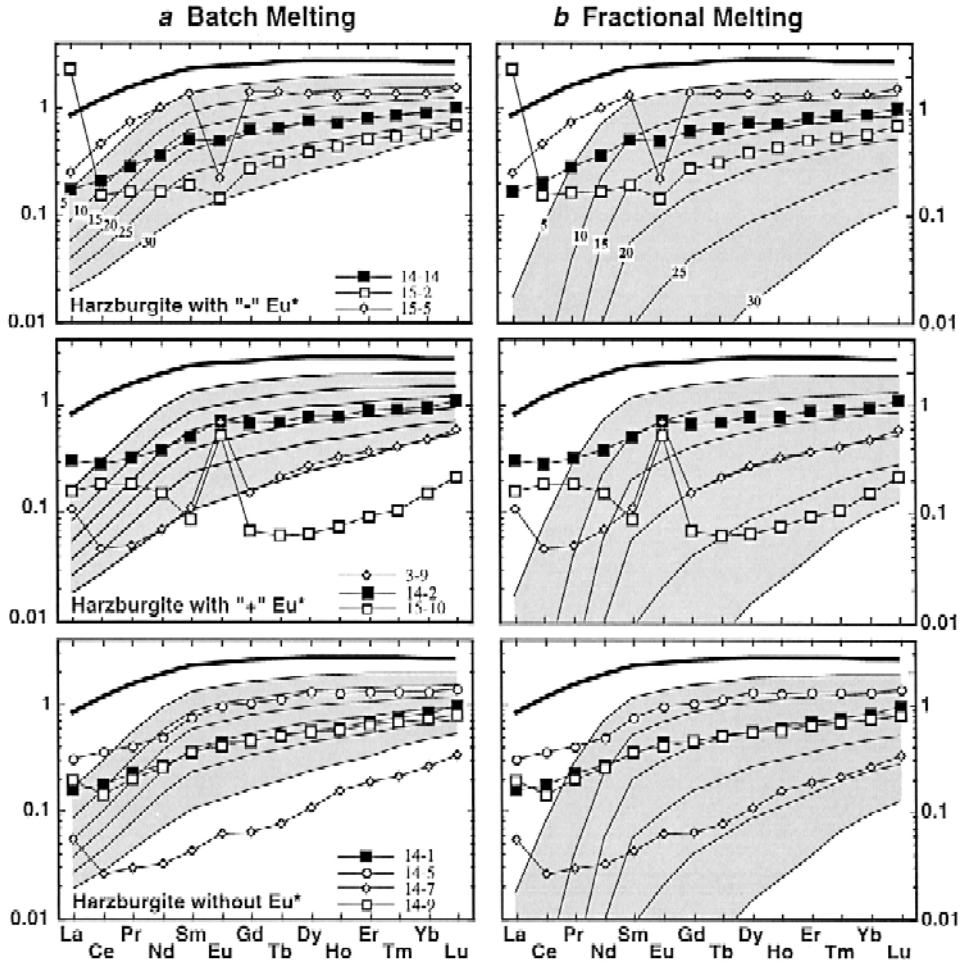

Fig. 6. Chondrite [42] normalized rare earth element abundances of Garrett harzburgites. For comparison, calculated depletion curves by (a) batch and (b) fractional melting models are also plotted. The model parameters are as for Fig. 2g–h. Note that the abundance levels and patterns are inconsistent with their being simple melting residues by either model, given their overall similarly depleted in residual mineral compositions (Fig. 4), but are consistent with melt refertilization. Also note that the anomalous La in GN3-9, 14-7, and 15-2 is interpreted as resulting from relative mobility of La during serpentinization.

chemically quite similar, it is difficult to explain the variable Nb/Ta ratios by chemical consideration alone. Because Nb and Ta have very different atomic masses, ^{93}Nb vs. ^{181}Ta (the superscripts are atomic masses), we propose that diffusion may control their apparent incompatibility. Heavier elements would diffuse slower than lighter ones, and would be even slower when the abundance level is extremely low (in residues) due to reduced compositional gradient across the mineral grains undergoing melting. This explains the curved Nb/Ta vs. Nb and Th trends (Fig. 8d,e) with large Nb/Ta changes in more depleted rocks [43]. The observation [43] that $^{90-92}$Zr is more incompatible than $^{177-180}$Hf, and ^{85,87}Rb is more incompatible than ^{133}Cs in highly depleted MORB can be explained likewise. The positive Th anomaly (relative to Nb) in the harzburgites may also be explained likewise (^{232}Th vs. ^{93}Nb; i.e., low

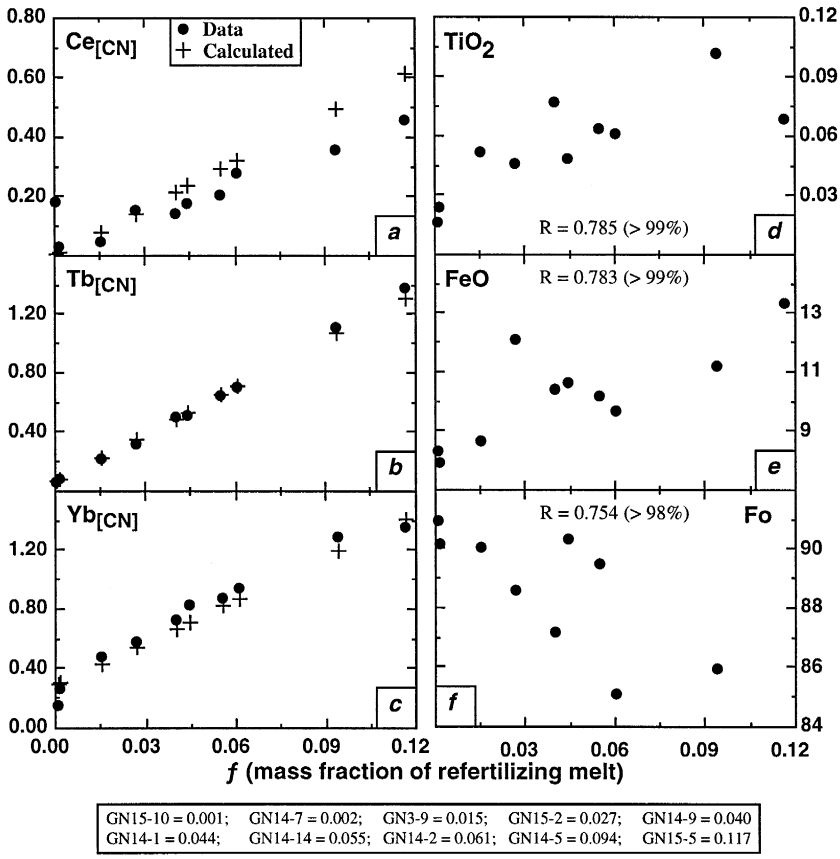

Fig. 7. (a)–(c) Comparisons between the data and calculated abundances ([CN], chondrite-normalized) of light (Ce), intermediate (Tb), and heavy (Yb) REE abundances. The calculation is done by adding various amounts (f) of a basaltic melt (M = GN4-11) to a residue (R = 25% fractional melting) by simultaneously solving the equation $f = (C_{Data} - C_R)/(C_M - C_R)$ for all, but La and Eu, REEs. Note that the fits are less good for light REEs given their more variable patterns for some samples (Fig. 6), but are excellent for intermediate and heavy REEs. (d)–(f) Plots of whole-rock TiO_2 and FeO, and olivine forsterite contents with the calculated f to show that these significant correlations are consistent with melt refertilization.

Nb/Th ratios) despite their different chemical properties.

5. Implications

5.1. What causes the high extents of melting beneath the EPR: a hot mantle or fast spreading rate?

We have shown that Garrett harzburgites are extremely depleted, as depleted as, or even more depleted than, abyssal peridotites from hotspot-influenced ridged in the Atlantic and Indian oceans (Fig. 4). In addition, recently drilled samples from Hess Deep [21], and our unpublished data from both Hess Deep and the Terevaka Transform [19] also are similarly depleted. One may interpret these highly depleted harzburgites as resulting from a depleted fertile mantle, but this requires that the observations at the three locations be fortuitous. Importantly, MORB from the broad EPR region are not highly depleted. Therefore, the highly depleted harzburgites from these locations are consistent with very high extents of melting ($\sim$ 25%). If the extent of melting relates in a simple way to mantle temperature variation [5,8], this would suggest a hotter EPR mantle. However, the EPR in this broad region has normal topography and morphology thermally unaffected by

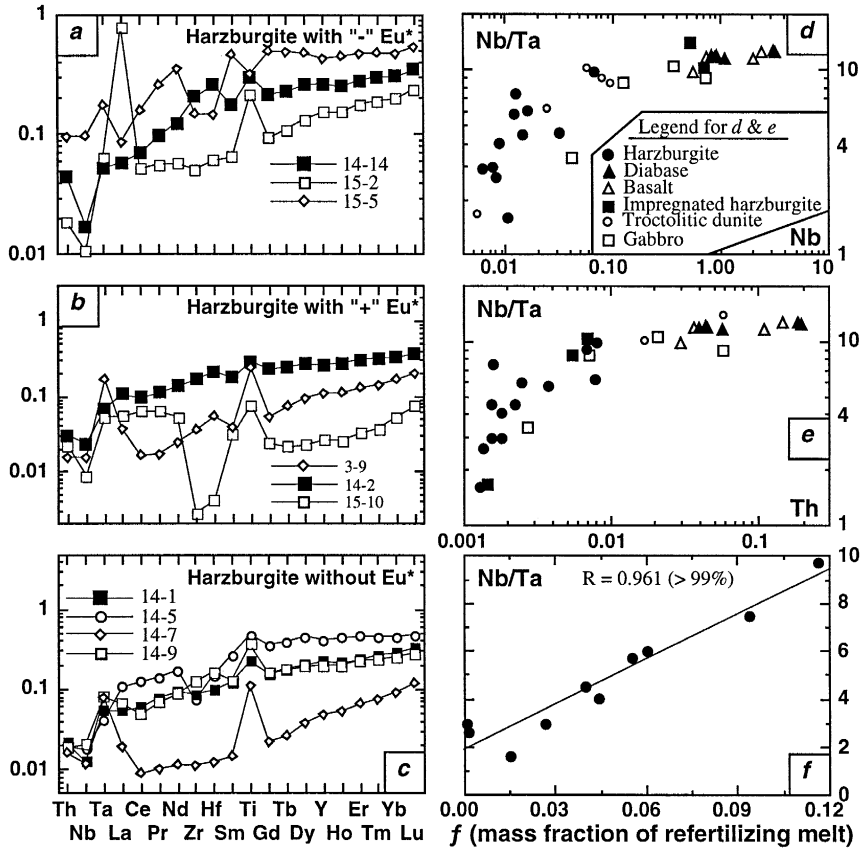

Fig. 8. (a)–(c) Primitive mantle [42] normalized incompatible element abundances in Garrett harzburgites to show some anomalous features about Ti, Zr, Hf, Nb, Ta and Th relative to REEs. (d) Plot of Nb/Ta vs. Nb of all the lithologies analyzed from the Garrett Transform to show that the curved trend is consistent with the observation that Nb is more incompatible than Ta [43,44]. (e) Plot of Nb/Ta vs. Th to show that Nb/Ta ratio in a rock increases with increasing incompatible element (e.g., Th) abundances. (f) The significant correlation between Nb/Ta ratio and the calculated refertilization parameter (Fig. 7) attests that the true melting residues would have Nb/Ta < 2, and the variably higher Nb/Ta ratios result from the refertilization process discussed in the text.

any known hotspots. Hence, factors other than mantle temperature variation may play a role. We propose that plate spreading rate variation may be as important as mantle temperature variation. The high extents of melting beneath the EPR may result from a fast spreading rate. Given the fact that mantle upwelling beneath ridges results from plate separation, fast separation leads to fast mantle upwelling [45–48]. Fast upwelling allows the adiabat to extend to shallower levels (i.e., against the conductive cooling to the seafloor), thus decompression melting continues up to a shallower level, and more melt forms from a given parcel of mantle.

That oceanic crustal thickness is generally constant, and is independent of plate spreading rate [49,50], has been the primary constraint leading to the idea that the extent of melting beneath ocean ridges is independent of spreading rate. However, the crustal thickness is entirely inferred from seismic data. The fact that thin crust and peridotite outcrops have been observed within axial zones at slow-spreading ridges but not at fast-spreading ridges

suggests that crustal thickness derived from seismic data must be used with caution [51]. The significant implications are: (1) the notion that MORB represent $\leq 10\%$ melting beneath global ocean ridges needs revision with the available peridotite data from the EPR; and (2) models on MORB genesis that neglect spreading rate variation need re-evaluation.

5.2. Do MORB melts experience low pressure equilibration during ascent?

Recent studies have led to the idea that melts formed at depth must be extracted rapidly without experiencing low-pressure equilibration during ascent [8]. The presence of excess olivine and incompatible element refertilization seen in Garrett harzburgites attest the significant melt–solid equilibration during melt ascent. As excess olivine is observed on petrographic scales in abyssal peridotites from slow-spreading ridges as well [52], porous flows may be as important as channel flows during melt migration. Therefore, melt–solid equilibration during melt ascent at shallow levels is unavoidable. Caution is thus necessary when inferring melting pressures from basalt chemistry, as has been pointed out in recent studies [53–55].

Acknowledgements

YN acknowledges support from The University of Queensland and from the Australian Research Council. RH acknowledges support from Ministere des Affairs Etrangeres in France as well as the Department of Marine Geosciences at IFREMER. Both YN and RH are grateful for the Bilateral Science and Technology Program of Australia and the Ministere de l'Education de l'enseignement Superieur et de la Recherche of France, without which this work would not have been completed. We thank Robyn Frankland and Kim Baublys for helping with sample preparations, Peter Colls for thin sections, and Frank Audsley for XRF analyses at the University of Queensland, and Marcel Bohn for assistance with the microprobe analysis at IFREMER. We are grateful for the constructive comments of Jon Snow and two anonymous reviewers. ***[FA]***

Appendix A. Rare earth element mineral / liquid partition coefficients used in this study

Kd values	Clino-pyroxene	Ortho-pyroxene	Spinel	Olivine
La	0.0560	0.0053	0.0003	0.0067
Ce	0.0920	0.0090	0.0005	0.0060
Pr	0.1610	0.0127	0.0007	0.0060
Nd	0.3030	0.0163	0.0008	0.0059
Sm	0.4450	0.0200	0.0009	0.0067
Eu	0.5005	0.0275	0.0010	0.0074
Gd	0.5560	0.0350	0.0011	0.0095
Tb	0.5700	0.0480	0.0013	0.0115
Dy	0.5820	0.0610	0.0018	0.0154
Ho	0.5825	0.0740	0.0023	0.0193
Er	0.5830	0.0838	0.0030	0.0256
Tm	0.5625	0.0935	0.0038	0.0374
Yb	0.5420	0.1033	0.0045	0.0491
Lu	0.5060	0.1130	0.0050	0.0600

Data from [63–67].

References

[1] H.J.B. Dick and R.L. Fisher, Mineralogic studies of the residues of mantle melting: Abyssal and alpine type peridotites, in: The Mantle and Crustal–mantle Relationships — Mineralogical, Petrological, and Geodynamic Processes, 3rd Int. Kimberlite Conf., II, J. Kompobst, ed., pp. 295–308, New York, NY, 1984.

[2] H.J.B. Dick, R.L. Fisher and W.B. Bryan, Mineralogical variability of the uppermost mantle along mid-ocean ridges, Earth Planet. Sci. Lett. 69, 88–106, 1984.

[3] P.J. Michael and E. Bonatti, Peridotite composition from the North Atlantic: Regional and tectonic variations and implications for partial melting, Earth Planet. Sci. Lett. 73, 91–104, 1985.

[4] K.T.M. Johnson, H.J.B. Dick and N. Shimizu, Melting in the oceanic upper mantle: an ion microprobe study of diopside in abyssal peridotites, J. Geophys. Res. 95, 2661–2678, 1990.

[5] E.M. Klein and C.H. Langmuir, Global correlations of ocean ridge basalt chemistry with axial depth and crustal thickness, J. Geophys. Res. 92, 8089–8115, 1987.

[6] D. McKenzie and M.J. Bickle, The volume and composition of melt generated by extension of the lithosphere, J. Petrol. 29, 625–679, 1988.

[7] Y. Niu and R. Batiza, An empirical method for calculating melt compositions produced beneath mid-ocean ridges: application for axis and off-axis (seamounts) melting, J. Geophys. Res. 96, 21,753–21,777, 1991.

[8] C.H. Langmuir, E.M. Klein and T. Plank, Petrological systematics of mid-ocean ridge basalts: Constraints on melt generation beneath ocean ridges, in: Mantle Flow and Melt Generation at Mid-ocean Ridges, J. Phipps Morgan, D.K. Blackman and J.M. Sinton, eds., AGU Geophys. Monogr. 71, 183–280, 1992.

[9] J.P. Brodholt and R. Batiza, Global systematics of unavenged mid-ocean ridge basalt compositions: Comments on ''Global correlations of ocean ridge basalt chemistry with axial depth and crustal thickness by E.M. Klein and C.H. Langmuir'', J. Geophys. Res. 94, 4231–4239, 1989.

[10] E.M. Klein and C.H. Langmuir, Local versus global variation in ocean ridge basaltic composition: A reply, J. Geophys. Res. 94, 4241–4252, 1989.

[11] R. Batiza, R. Hékinian, D. Bideau and J. Francheteau, Chemistry of deep (3500–5600 m) Pacific MORB — Why is the Pacific anomalous?, Geophys. Res. Lett. 22, 3067–3070, 1995.

[12] Y. Niu and R. Batiza, Chemical variation trends at fast and slow spreading ridges, J. Geophys. Res. 98, 7887–7902, 1993.

[13] Yu.P. Neprochnov and G.L. Kashintsev, Composition of the main crustal layers of the East Pacific Rise, Oceanology 239, 199–201, 1978.

[14] H. Bäcker, J. Lange and V. Marchig, Hydrothermal activity and sulfide formation in axial valleys of the East Pacific Rise crest between 18°S and 22°S, Earth Planet. Sci. Lett. 72, 9–22, 1985.

[15] J. Francheteau, R. Armijo, J.L. Cheminée, R. Hékinian, P. Lonsdale and N. Blum, 1 Ma East Pacific Rise oceanic crust and upper mantle exposed by rifting in Hess deep (equatorial Pacific Ocean), Earth Planet. Sci. Lett. 101, 282–295, 1990.

[16] R. Hékinian, D. Bideau, J. Franchteau, J.J. Cheminee, R. Armijo, P. Lonsdale and N. Blum, Petrology of the East Pacific Rise crust and upper mantle exposed in Hess Deep (eastern equatorial Pacific), J. Geophys. Res. 98, 8069–8094, 1993.

[17] R. Hékinian, D. Bideau, M. Cannat, J. Franchteau and R. Hébert, Volcanic activity and crust–mantle exposure in the ultrafast Garrett transform fault near 13°28′S in the Pacific, Earth Planet. Sci. Lett. 108, 259–273, 1992.

[18] R. Hékinian, D. Bideau, R. Herbért and Y. Niu, Magmatism in the Garrett transform (East Pacific Rise near 13°27′S), J. Geophys. Res. 100, 10,163–10,185, 1995.

[19] M. Constantin, R. Hékinian, D. Ackermand and P. Stoffers, Mafic and ultramafic intrusions into upper mantle peridotites from fast spreading centers of the Easter microplate (Southeast Pacific), in: Mantle and Lower Crust Exposed in Oceanic Ridges and Ophiolites, R.L.M. Visser and A. Nicolas, eds., pp. 71–120, Kluwer, Dordrecht, 1995.

[20] R. Hékinian, R. Armijo, J.P. Cogné, M. Constantin, J. Francheteau, J. Girardeau, R.N. Hey, D.F. Naar and R. Searle, Petrology of the Easter microplate region in the south Pacific, J. Geophys. Res., submitted, 1996.

[21] H.J.B. Dick and J.H. Natland, Late stage melt evolution and transport in the shallow mantle beneath the East Pacific Rise, Proc. ODP Sci. Results 147, 103–134, 1996.

[22] C. DeMets, R.G. Gordon, D.F. Argus and S. Stein, Current plate motions, Geophys. J. Int. 101, 425–478, 1990.

[23] P. Lonsdale, Segmentation of the Pacific–Nazca spreading center, 1°N–20°S, J. Geophys. Res. 94, 12,179–12,225, 1989.

[24] R. Batiza, B.R. Rosendahl and R.L. Fisher, Evolution of ocean crust 3, Petrology and geochemistry of basalts from the East Pacific Rise and Siqueiros transform fault, J. Geophys. Res. 82, 265–276, 1977.

[25] R. Hébert, D. Bideau and R. Hékinian, Ultramafic and mafic rocks from the Garrett Transform fault near 13°30′N on the East Pacific Rise: igneous petrology, Earth Planet. Sci. Lett. 65, 107–125, 1983.

[26] M. Cannat, D. Bideau and R. Hébert, Plastic deformation and magmatic impregnation in serpentinized ultramafic rocks from the Garrett transform fault (East Pacific Rise), Earth Planet. Sci. Lett. 101, 216–232, 1990.

[27] K. Norrish and J.T. Hutton, J.T. An accurate X-ray spectrographic method for the analysis of a wide range of geological samples, Geochim. Cosmochim. Acta 33, 431–453, 1968.

[28] Y. Tao, P.A. Pella and R.M. Rousseau, NBSGSC — a FORTRAN program for quantitative X-ray fluorescence analysis, NBS Techn. Note 1213, 1985.

[29] H.J.B. Dick, Abyssal peridotites, very slow spreading ridges and ocean ridge magmatism, in: Magmatism in the Ocean Basins, A.D. Saunders and M.J. Norry, eds., Geol. Soc. London Spec. Publ. 42, 71–105, 1989.

[30] K.T.M. Johnson and H.J.B. Dick, Open system melting and the temporal and spatial variation of peridotite and basalt compositions at the Atlantis II F.Z., J. Geophys. Res. 97, 9219–9241, 1992.

[31] D.R. Janecky and W.E. Seyfried, Hydrothermal serpentinization of peridotite within the oceanic crust: Experimental investigations of mineralogy and major element chemistry, Geochim. Cosmochim. Acta 50, 1357–1378, 1986.

[32] A.L. Jaques and D.H. Green, Anhydrous melting of peridotite at 0–15 kb pressure and the genesis of tholeiitic basalts, Contrib. Mineral. Petrol. 73, 287–310, 1980.

[33] H.J.B. Dick and T.B. Bullen, Chromian spinel as a petrogenetic indicator in abyssal and alpine-type peridotites and spatially associated lavas, Contrib. Mineral. Petrol. 86, 54–76, 1984.

[34] E.M. Klein, T. Plank and C.H. Langmuir, Constraints on models for mantle melting beneath ocean ridges, RIDGE Events 2, 11–12, 1991.

[35] D.W. Forsyth, Crustal thickness and the average depth and degree of melting in fractional melting models of passive flow beneath mid-ocean ridges, J. Geophys. Res. 98, 16,073–16,079, 1993.

[36] W.F. McDonough, H.-G. Stosch and N.G. Ware, Distribution of titanium and the rare earth elements between peridotitic minerals, Contrib. Mineral. Petrol. 110, 321–328, 1992.

[37] E. Rampone, A.W. Hofmann, G.B. Piccardo, R. Vannucci, P. Bottazzi and L. Ottolini, Trace element and isotope geochemistry of depleted peridotites from an N-MORB type ophiolite (Internal Liguride, N. Italy), Contrib. Mineral. Petrol. 123, 61–76, 1996.

[38] A.V. Sobolev, and N. Shmizu, Ultra-depleted primary melt

included in an olivine from the Mid-Atlantic Ridge, Nature 363, 151–154, 1993.
[39] A.V. Sobolev, A.A. Gurenko and N. Shmizu, Ultra-depleted melts from Iceland: data from melt inclusion studies, Mineral. Mag. 58A, 860–861, 1994.
[40] H. Bougault, J.-L. Joron and M. Treuil, Alteration, fractional crystallization, partial melting, mantle properties from trace elements in basalts recovered in the North Atlantic, in: Deep Drilling Results in the Atlantic Ocean: Ocean Crust, M. Talwani, C.G. Harrison and D.E. Hayes, eds., pp. 352–367, 1979.
[41] A.W. Hofmann, Chemical differentiation of the Earth: the relationship between mantle, continental crust, and oceanic crust, Earth Planet. Sci. Lett. 90, 297–314, 1988.
[42] S.-S. Sun and W.F. McDonough, Chemical and isotopic systematics of ocean basalt: Implications for mantle composition and processes, in: Magmatism of the Ocean Basins, A.D. Saunders and M.J. Norry, eds., Geol. Soc. London Spec. Publ. 42, 323–345, 1989.
[43] Y. Niu and R. Batiza, Extreme mantle source heterogeneities beneath the northern East Pacific Rise — trace element evidence from near ridge seamounts, EOS Trans. AGU 76, F595, 1995.
[44] T. Plank and W.M. White, Nb and Ta in Arc and mid-ocean ridge basalts, EOS Trans. AGU 76, F655, 1995.
[45] Y. Bottinga and C.J. Allègre, partial melting under spreading ridges, Philos. Trans. R. Soc. London A 288, 501–525, 1978.
[46] I. Reid and H.R. Jackson, Oceanic spreading rate and crustal thickness, Mar. Geophys. Res. 5 165–172, 1981.
[47] D.W. Forsyth, Geophysical constraints on mantle flow and melt generation beneath mid-ocean ridges, in: Mantle Flow and Melt Generation at Mid-ocean Ridges, J.P. Morgan, D.K. Blackman and J.M. Sinton, eds., AGU Geophys. Monogr. 71, 1–66, 1992.
[48] D.L. Turcotte and J. Phipps Morgan, Magma migration and mantle flow beneath a mid-ocean ridge, in: Mantle Flow and Melt Generations Beneath Mid-Ocean Ridges, J. Phipps Morgan, D.K. Blackman and J.M. Sinton, eds., AGU Geophys. Monogr. 71, 155–182, 1993.
[49] Y.J. Chen, Oceanic crustal thickness versus spreading rate, Geophys. Res. Lett. 19, 753–756, 1992.
[50] J.W. Bown and R.S. White, Variation with spreading rate of oceanic crustal thickness and geochemistry, Earth Planet. Sci. Lett. 121, 435–449, 1994.
[51] M. Cannat, How thick is the magmatic crust at slow spreading ridges?, Geophys. Res. 101, 2847–2857, 1996.
[52] Y. Niu, Mantle melting processes beneath slow-spreading ocean ridges: evidence from abyssal peridotites, J. Petrol., submitted, 1996.
[53] J.H. Natland, Partial melting of a lithologically heterogeneous mantle: Inferences from crystallisation histories of magnesian abyssal tholeiites from the Siqueiros Fracture Zone, in: Magmatism in Ocean Basins, A.D. Saunders and M.J. Norry, eds., Geol. Soc. London Spec. Publ. 42, 41–70, 1989.
[54] F. Albarède, How deep do common basaltic magmas form and differentiate?, J. Geophys. Res. 97, 10,997–11,009, 1992.
[55] Y. Shen and D.W. Forsyth, Geochemical constraints on initial and final depth of melting beneath mid-ocean ridges, J. Geophys. Res. 100, 2211–2237, 1995.
[56] P.L. Roeder and R.F. Emslie, Olivine–liquid equilibrium, Contrib. Mineral. Petrol. 29, 275–289, 1970.
[57] F.A. Frey, C.J. Suen and H. Stockman, The Ronda high temperature peridotite: Geochemistry and petrogenesis, Geochim. Cosmochim. Acta 49, 2469–2491, 1985.
[58] M.B. Baker and E.M. Stolper, Determining the composition of high-pressure mantle melts using diamond aggregates, Geochim. Cosmochim. Acta 58, 2811–2827, 1994.
[59] J.E. Snow and H.J.B. Dick, Pervasive magnesium loss by marine weathering of peridotite, Geochim. Cosmochim. Acta 59, 4219–4235, 1995.
[60] T. Shibata and G. Thompson, Peridotites from the mid-Atlantic ridge at 43°N and their petrogenetic relation to abyssal tholeiites, Contrib. Mineral. Petrol. 93, 144–159, 1986.
[61] M. Cannat, D. Bideau and H. Bougault, Serpentinized peridotites and gabbros in the Mid-Atlantic Ridge axial valley at 15°37′N and 16°52′N, Earth Planet. Sci. Lett. 109, 87–106, 1992.
[62] H. Bougault, L. Dmitriev, J.-G. Schilling, A. Sobolev, J.L. Joron and H.D. Needham, Mantle heterogeneity from trace elements, MAR triple junction near 14°N, Earth Planet. Sci. Lett. 88, 27–36, 1988.
[63] A.J. Irving, A review of experimental studies of crystal liquid trace element partitioning, Geochim. Cosmochim. Acta 42, 743–770, 1978.
[64] T.H. Green, S.H. Sie, C.G. Ryan and D.R. Cousens, Proton microprobe determined partitioning of Nb, Ta, Zr, Sr, and Y between garnet, clinopyroxene and basaltic magma at high pressure and temperature, Chem. Geol. 74, 201–216, 1989.
[65] G.A. McKay, Crystal/liquid partitioning in basaltic systems: Extreme fractionation of REE in olivine, Geochim. Cosmochim. Acta 50, 69–79, 1986.
[66] W.E. Graham and R.L. Nielson, The partitioning of Sc, Y, and the rare earth elements between high-Ca pyroxene and natural mafic to intermediate lavas at one atmosphere, Geochim. Cosmochim. Acta 56, 2387—2404, 1992.
[67] H. Fujimaki, M. Tatsumoto and K. Aoki, Partition coefficients of Hf, Zr, and REE betwen phenocrysts and groundmass, Proc. Lunar Planet. Sci. Conf. 14, part 2, J. Geophys. Res. 89, suppl. B662–B672, 1984.